

Monte Carlo Test of the Classical Theory for Heterogeneous Nucleation Barriers

David Winter, Peter Virnau, K. Binder
*Institut für Physik, Johannes Gutenberg-Universität,
 D-55099 Mainz, Staudinger Weg 7, Germany*
 (Dated: February 14, 2022)

Flat walls facilitate the condensation of a supersaturated vapor: Classical theory of heterogeneous nucleation predicts that the free energy barrier ΔF_{het}^* which needs to be overcome for the formation of sphere-cap shaped nucleation seeds is smaller than the barrier ΔF_{hom}^* for spherical droplets in the bulk by a factor $0 < f(\theta) < 1$, which only depends on the contact angle θ . In this letter we compute both ΔF_{hom}^* and ΔF_{het}^* from Monte Carlo simulations and test the theory for the lattice gas model (for which θ can be readily controlled). Even though the theory is only based on macroscopic arguments, it is shown to hold for experimentally relevant nanoscopic nucleation seeds ($20 \leq \Delta F_{\text{hom}}^*/k_B T \leq 200$) if (independently estimated) line tension effects are considered.

PACS numbers: 64.60.an, 64.60.Q-, 64.70.F-, 68.08.Bc

Nucleation [1–5] is a ubiquitous process which governs such diverse phenomena as the formation of rain drops or snow flakes in the atmosphere, the crystallization of proteins and even the formation of industrially relevant polymer foams. Even though considerable empirical knowledge has been gathered, e.g., on which materials are suited as seed particles for making clouds rain [6] or as nucleation agents to start precipitation in metallurgy [7], many questions remain. Reasons for this partial shortcoming are manifold: Experiments are very difficult to control. Homogeneous nucleation in the bulk needs to be separated from heterogeneous nucleation at walls or impurities, and small changes in parameters typically lead to large changes in corresponding nucleation rates. Nucleation sites often only consist of a few hundred or thousand atoms and can only be observed indirectly. Unfortunately, theoretical progress is also hampered by these difficulties. Simulations on the other hand offer full control and are at least in principle able to bridge the gap between theory and experiment and, indeed, significant progress has been achieved in recent years [8–10].

According to Classical Nucleation Theory [1, 2], the formation of a (spherical) nucleation seed in the bulk is understood in terms of two competing factors: a volume term which seeks to expand the seed and an opposing surface term $F_s = 4\pi R^2 \gamma$:

$$\Delta F(R) = -\Delta\mu(\rho_l - \rho_v) \frac{4\pi R^3}{3} + 4\pi R^2 \gamma. \quad (1)$$

R is the radius of the droplet (or bubble), γ the interfacial tension (of a macroscopically flat interface), $\Delta\mu = \mu - \mu_{\text{coex}}$ the difference in chemical potential relative to the coexistence value, and $\rho_{l,v}$ the densities of the coexisting phases. The free energy barrier ΔF^* can now be obtained by determining the maximum of Eq. (1) at R^* . Interestingly, at R^* we also obtain

$$\Delta F^* = \frac{1}{3} F_s(R^*). \quad (2)$$

Hence, the nucleation barrier can directly be inferred

from the knowledge of the surface free energy of a droplet or bubble. Note that the spontaneous formation of a critical nucleus of the new phase in the bulk requires a free energy barrier ΔF_{hom}^* of the order $20 \leq \Delta F_{\text{hom}}^*/k_B T \leq 200$. Compared to thermal fluctuations (that one can easily detect e.g. by scattering experiments) this is a rare event.

The presence of a wall facilitates nucleation and reduces the barrier. For macroscopic droplets (see Fig. 1), the contact angle θ between the droplet and the wall is given by the competition of the vapor-liquid (γ_{vl}), wall-vapor (γ_{wv}) and wall-liquid (γ_{wl}) interface free energies [11]

$$\gamma_{vl} \cos \theta = \gamma_{wv} - \gamma_{wl}, \quad (3)$$

for incomplete wetting conditions ($\gamma_{vl} > \gamma_{wv} - \gamma_{wl}$) [12]. Eq. (3) is known as Young's equation and can be derived by considering the forces acting at the three phase boundary. For small droplets, a correction due to the line tension (τ) of the contact line arises [13] (which has the length $2\pi r$, where $r = R \sin \theta$).

Considering Eq. (3) and the geometry of the sphere-cap (see caption of Fig. 1) we obtain Turnbull's estimate for the surface free energy [13–15]:

$$F_{s,\text{het}} = F_{s,\text{hom}} \cdot f(\theta), \\ f(\theta) = (1 - \cos \theta)^2 (2 + \cos \theta) / 4. \quad (4)$$

Intriguingly, $f(\theta) = V_{\text{sphere-cap}}/V_{\text{droplet}}$. Therefore, Eq. (2) also holds for the heterogeneous case and we get:

$$\Delta F_{\text{het}} = \Delta F_{\text{hom}} \cdot f(\theta). \quad (5)$$

The nucleation barrier in the heterogeneous case is simply reduced by a factor of $f(\theta)$. Note that this derivation is solely based on macroscopic considerations and has to our knowledge never actually been tested. In this letter we will demonstrate with Monte Carlo simulations of an Ising lattice gas model that this formula can be applied to nanoscopic systems if line tension effects are

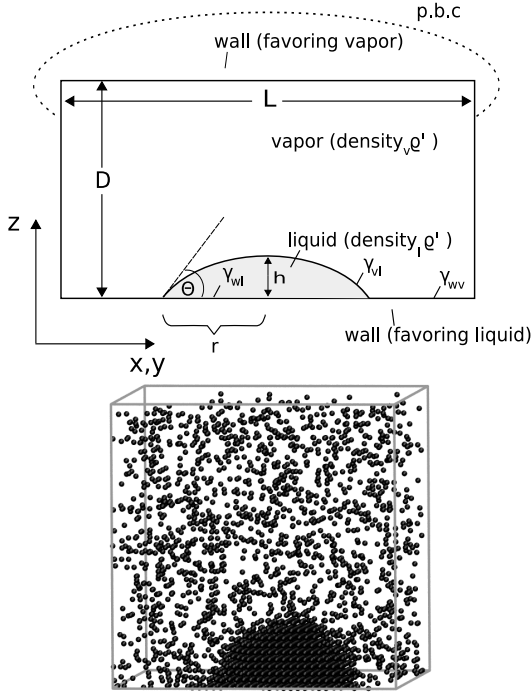


FIG. 1: a) Schematic drawing of the system which we use to study stable wall-attached droplets in thermal equilibrium. The sphere-cap shaped droplet has height h and covers a circle of radius r at the wall, with $r = R \sin \theta$, $h = R(1 - \cos \theta)$. R denotes the radius of curvature and θ the contact angle. For $R < \infty$, the density ρ_v of the vapor which coexists with the liquid droplet (at the same chemical potential $\mu > \mu_{\text{coex}}$) exceeds ρ_v (Gibbs-Thomson effect [13, 14]). b) Typical snapshot picture of a lattice gas system at $k_B T/J = 3.0$, $\rho = 0.065$, $L = D = 40$ (measured in units of the lattice spacing), and $H_1/J = 0$ ($\theta = 90^\circ$). Occupied lattice sites are highlighted by dots.

considered. This provides a stringent test for both the classical theory of homogeneous and heterogeneous nucleation. For this purpose we propose a new method [16, 17] to measure surface free energies (and hence nucleation barriers) of liquid droplets in the bulk and of droplets attached to walls over the experimentally relevant range. No “atomistic” identification of which particles belong to the droplet and which to the vapor is required. No bias potential to stabilize droplets of a particular size [8] is needed, and fluctuations of the droplet are not constrained. We independently determine the droplet volume and the chemical potential that characterizes the (*stable*) equilibrium between the small droplet and surrounding vapor in the *finite system* and derive an expression for the line tension.

We test Turnbull’s formula (5) with Monte Carlo simulations of the standard nearest neighbor (Ising) lattice gas model on the simple cubic lattice: $\mathcal{H} = -J \sum S_i S_j$, $S_{i,j} = \pm 1$. Phase coexistence between saturated vapor at density ρ_v and liquid ρ_ℓ occurs at a (known) chemical potential μ_{coex} . (In magnetic nota-

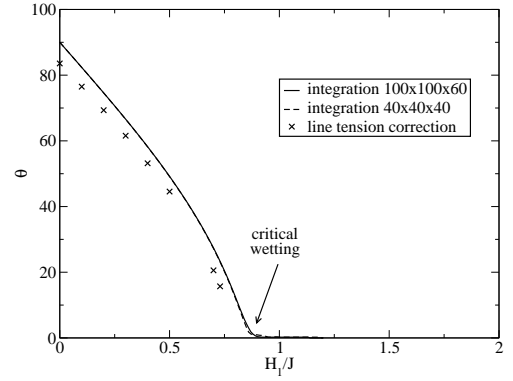


FIG. 2: Contact angle θ as derived from Eq. (6) plotted vs. H_1/J at $k_B T/J = 3.0$ for two lattice sizes (full and broken curves). Symbols show the prediction if the estimates for τ from our analysis of the droplet excess free energies and $r = 5$ are considered (see below).

tion, the magnetic field $H = (\mu - \mu_{\text{coex}})/2$, and ρ_ℓ , ρ_v are related to the spontaneous magnetization m_{coex} as $\rho_v = (1 - m_{\text{coex}})/2$, $\rho_\ell = (1 + m_{\text{coex}})/2$.) Bulk systems are studied in cubic simulation boxes with periodic boundary conditions in all directions. For the heterogeneous case we choose a $L \times L \times D$ geometry with periodic boundary conditions in x and y direction. Surface fields H_1 and $H_D = -H_1$ act on (the first layer of) the two free $L \times L$ surfaces. The temperature is set to $k_B T/J = 3.0$ to stay away from the bulk critical temperature (at $k_B T/J \approx 4.51$) and above the roughening transition temperature [18] (at $k_B T/J \approx 2.45$). Hence, the correlation length ξ is less than a lattice spacing and the interface free energy does (to a good approximation) not depend on the interface orientation.

Wetting for the Ising model has been thoroughly studied before [19] and by varying the surface field H_1 we can control the contact angle (Fig. 2). Note that the local surface layer magnetization $m_1 = -(\partial f_s(T, H, H_1)/\partial H_1)_{T,H}$ [20] (f_s is the surface excess free energy per spin). With $f_s(T, H \rightarrow 0^-, H_1) = \gamma_{wv}$, $f_s(T, H \rightarrow 0^+, H_1) = \gamma_{wl}$ and Young’s equation (3), we obtain θ from thermodynamic integration

$$\cos \theta = (1/\gamma_{v\ell}) \int_0^{H_1} (m_D - m_1) dH'_1. \quad (6)$$

Here, we exploit the Ising symmetry $f_s(T, H \rightarrow 0^-, H_1) = f_s(T, H \rightarrow 0^+, -H_1)$ to use the local magnetization m_D at the other surface at which $H_D = -H_1$ acts. $\gamma_{v\ell} = 0.434$ was given by the very accurate estimates of Hasenbusch and Pinn [21].

In the following we describe how to obtain the surface free energy as a function of the droplet radius. First, we measure the chemical potential (in the canonical ensemble) as a function of density (Fig. 3) by applying an

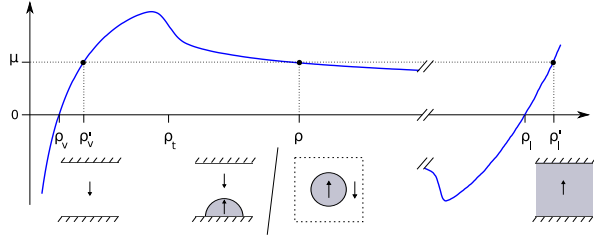


FIG. 3: Chemical potential as a function of density. The density of the sphere-cap shaped droplet at overall density ρ is given by ρ'_l , the density of the environment by ρ'_v . ΔF_s is obtained by integrating the chemical potential over the density from ρ'_v to ρ .

adaptation [16, 17] of the Widom test particle insertion method [22]. In the flat region of the isotherm depicted in Fig. 3, a single droplet is present in the simulation box, which will be used for the determination of the surface free energy. At small densities the ascending branch of μ represents pure vapor (with no single large droplet being present), and the subsequent rapid decrease signifies the system size dependent transition towards a single droplet phase [23–26]. At larger densities, the droplet region is delimited by a transition towards a cylindrical droplet which is stabilized by the boundary conditions. Note that for each system size, only a certain range of droplet sizes can be stabilized and we have to simulate a whole range of box sizes to cover all radii.

As indicated in Fig. 3 for each droplet state at density ρ , there exists one vapor state at ρ'_v and one liquid state at ρ'_l which have the same chemical potential. Equilibrium conditions require that the chemical potential is constant throughout the box. Therefore, the droplet has density ρ'_l and is surrounded by an environment with density ρ'_v . The surface free energy of the droplet is simply given by the difference in free energy between the droplet and the vapor state and can be determined by thermodynamic integration:

$$F_s(\rho) = \int_{\rho'_v}^{\rho} \mu(\rho') d\rho'. \quad (7)$$

The number of particles in the box is conserved:

$$\rho'_v(V - V_{drop}) + \rho'_l V_{drop} = \rho V. \quad (8)$$

If we further require that the (average) droplet is spherical in the bulk and sphere-cap shaped for the heterogeneous case, V_{drop} becomes $4/3\pi R^3$ or $4/3\pi R^3 f(\theta)$, respectively, and we obtain $R(\rho)$ and finally $F_s(R)$ and $F_s(R, \theta)$.

Fig. 4 a highlights the main results of our study. For the bulk we can directly test the classical theory of homogeneous nucleation by comparing our simulation results for $F_s(R)$ with the capillarity approximation

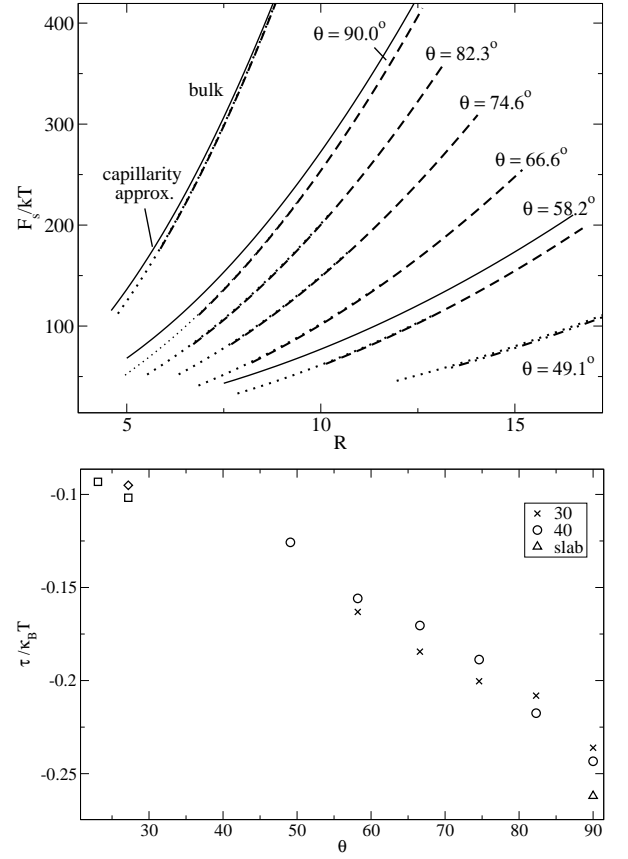


FIG. 4: a) Plot of $F_s(R, \theta)/k_B T$ vs. R for $k_B T/J = 3.0$ and a broad range of values for θ . Dotted lines are results for $L = D = 30$, dashes lines for $D = L = 40$, dash-dotted lines for $L = 60, D = 20$. For the systems (bulk, $H_1/J = 0$ and $H_1/J = 0.4$ ($\theta \approx 58^\circ$)) the classical predictions $4\pi R^2 \gamma_{vl}$ and $4\pi R^2 \gamma_{vl} f(\theta)$ are included (full curves). b) Plot of τ vs. θ for $k_B T/J = 3.0$. Crosses are data for $D = L = 30$, circles for $D = L = 40$, diamonds $D = 10, L = 60$, and squares for $D = 10, R = 80$.

$F_{c,bulk}(R) = 4\pi R^2 \gamma_{vl}$ [16, 26] (γ_{vl} being the interfacial tension for a flat interface.) For $R = 5$ the difference between the theoretical estimate and our simulation results is already less than 5% (at $k_B T/J = 3.0$) and quickly vanishes with increasing droplet radius. The validity of the capillarity approximation for the bulk agrees with conclusions drawn from surface force measurements on liquid bridges [29], but contrasts a large body of other work (see [26] for a discussion).

We have also determined the surface free energy for a sphere-cap shaped droplet attached to the wall for several contact angles as a function of the radius of curvature. It is important to note that within statistical errors different choices of L and D yield identical results. For $\theta = 90^\circ$ and $\theta = 58.2^\circ$ we have also included the theoretical estimate from the capillarity approximation $F_{c,hel} = F_{c,bulk} \cdot f(\theta)$. When we consider $F_{c,hel}(R, \theta) - F_s(R, \theta)$, we find that the difference in-

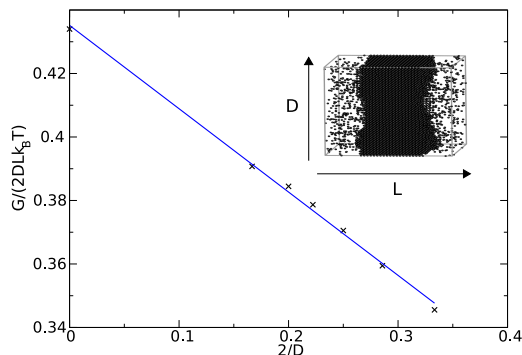


FIG. 5: Plot of the thermodynamic potential G for slab configurations (insert), normalized by temperature and total surface area $2LD$, versus $2/D$ so that the slope yields the line tension ($\tau/k_B T = 0.26 \pm 0.001$). The intercept of the ordinate was fixed to the literature value of the interface tension 0.434 [21].

creases linearly with R , and hence can be interpreted as a line tension contribution, $2\pi r\tau$. I.e., Eq (4) is modified to $F_{s,het} = F_{s,hom} \cdot f(\theta) + 2\pi r\tau$. This division of surface and line contributions relies on our droplet definition, Eq (8), which uses the fact that for the lattice gas the Tolman length [3–5] is zero. Fig. 4b shows a plot of the line tension τ obtained in this way versus contact angle. The line tension is negative, and becomes very small (and presumably vanishes) as $\theta \rightarrow 0$. The estimates for τ have been used (together with the appropriate estimates for R) in Fig. 2, to show the expected deviation of the contact angle for small droplets from the bulk value. An independent check of the line tension is obtained for $\theta = 90^\circ$ by investigating slab configurations (Fig.5) with varying D . In this case the potential can be written as $G/(2DLk_B T) = \gamma_{lv} + 2\tau/D$, and the slope in Fig.5 agrees with the estimate shown in Fig.4b. Hence, Eqs. (4) and (5) hold if a correction due to line tension is considered. Interestingly, an experimental hint for the need of a negative line tension describing bubble formation in water extrusion from mesopores was given in [30].

In summary, we have shown that the classical theory of heterogeneous nucleation at flat walls, which predicts a reduction of the free energy barrier by a factor $f(\theta)$, can describe the actual surface free energies $F_s(R, \theta)$, provided a line tension term is included into the latter. While the importance of line tension effects on small nuclei has been stressed in various other contexts, e.g. [9, 27, 28], the present paper is the first approach which provides a systematic method to obtain both $F_s(R)$ for spherical droplets in the bulk and $F_s(R, \theta)$ for wall-attached droplets, as well as for the contact angle θ and line tension τ . Thus, for the first time we verify Turnbull's equation from 1950, which still stands as one of the cornerstones of the theory of heterogeneous nucleation. The methods, which in this letter are described for the simple Ising model, can readily be generalized to

various models in broad classes of systems. They will enable significant progress in the understanding of nucleation phenomena in diverse branches of physics.

-
- [1] M. Volmer and A. Weber, Z. Chem. Phys. **119**, 277 (1926)
 - [2] A.C. Zettlemoyer (ed) *Nucleation* (M. Dekker, New York, 1969)
 - [3] K. Binder and D. Stauffer, Adv. Phys. **25**, 343 (1976)
 - [4] P. Debenedetti: *Metastable Liquids* Princeton University Press, Princeton (1997)
 - [5] D. Kashchiev: *Nucleation: Basic Theory with Applications* (Butterworth-Heinemann, Oxford, 2000)
 - [6] J. Curtius, Compt. Rendus Phys. **7**, 1027 (2006)
 - [7] H. Biloni, in *Physical Metallurgy* (R.W. Cahn and P. Haasen, eds.) North-Holland, Amsterdam (1983), p. 477
 - [8] P.R. Ten Wolde and D. Frenkel, J. Chem. Phys. **109**, 9901 (1998)
 - [9] S. Auer and D. Frenkel, Phys. Rev. Lett. **91**, 015703 (2003)
 - [10] L. Maibaum, Phys. Rev. Lett. **101**, 256102 (2008)
 - [11] T. Young, Phil. Trans. Roy. Soc. London **95**, 65 (1805)
 - [12] P.G.de Gennes, F. Brochard-Wyart, and D. Quéré, *Capillary and Wetting Phenomena: Drops, Bubbles, Pearls, Waves* (Springer, Berlin 2004)
 - [13] R.D. Gretz, J. Chem. Phys. **45**, 3160 (1966)
 - [14] D. Turnbull, J. Chem. Phys. **18**, 198 (1950); J. Appl. Phys. **21**, 1022 (1950)
 - [15] G. Navascues and P. Tarazona, J. Chem. Phys. **75**, 2441 (1981)
 - [16] D. Winter, P. Virnau, and K. Binder (in preparation)
 - [17] D. Winter, *Diplomarbeit* (Johannes Gutenberg-Universität Mainz, 2009, unpublished)
 - [18] K.K. Mon, S. Wansleben, D.P. Landau, and K. Binder, Phys. Rev. **B39**, 7089 (1989)
 - [19] K. Binder and D. P. Landau, Phys. Rev. **B37**, 1745 (1988); K. Binder, D.P. Landau and S. Wansleben, Phys. Rev. **B40**, 6971 (1989)
 - [20] K. Binder and P.C. Hohenberg, Phys. Rev. **B6**, 3461 (1972)
 - [21] M. Hasenbusch, and K. Pinn, Physica **A192**, 342 (1993); *ibid* **203**, 189 (1994)
 - [22] B. Widom, J. Chem. Phys. **39**, 2808 (1963)
 - [23] M. Biskup, L. Chayes and R. Kotecky, Europhys. Lett. **60**, 21 (2002)
 - [24] K. Binder, Physica **A319**, 99 (2003)
 - [25] L.G. MacDowell, P. Virnau, M. Müller, and K. Binder, J. Chem. Phys. **120**, 5293 (2004)
 - [26] M. Schrader, P. Virnau, and K. Binder, Physical Review **E 79**, 061104 (2009)
 - [27] A. Milchev, and K. Binder, J. Chem. Phys. **114**, 8610 (2001)
 - [28] S. Mechkov, G. Oshanin, M. Rauscher, M. Brinkmann, A.M. Cazabtat and S. Dietrich, Europhys. Lett. **80**, 66002 (2007)
 - [29] J. Crassous, E. Charlaix, J.L. Loubet, Europhys. Lett. **28**, 37 (1994)
 - [30] B. Lefevre, A. Saugey, J.L. Barrat, et al., J. Chem. Phys. **120**, 4927 (2004)